Science Advances
AAAS

advances.sciencemag.org/cgi/content/full/6/35/eabb1573/DC1

Supplementary Materials for

Highly active dry methane reforming catalysts with boosted in situ grown Ni-Fe nanoparticles on perovskite via atomic layer deposition

Sangwook Joo, Arim Seong, Ohhun Kwon, Kyeounghak Kim, Jong Hoon Lee, Raymond J. Gorte, John M. Vohs*, Jeong Woo Han*, Guntae Kim*

*Corresponding author. Email: vohs@seas.upenn.edu (J.M.V.); jwhan@postech.ac.kr (J.W.H.); gtkim@unist.ac.kr (G.K.)

Published 26 August 2020, *Sci. Adv.* **6**, eabb1573 (2020)
DOI: 10.1126/sciadv.abb1573

This PDF file includes:

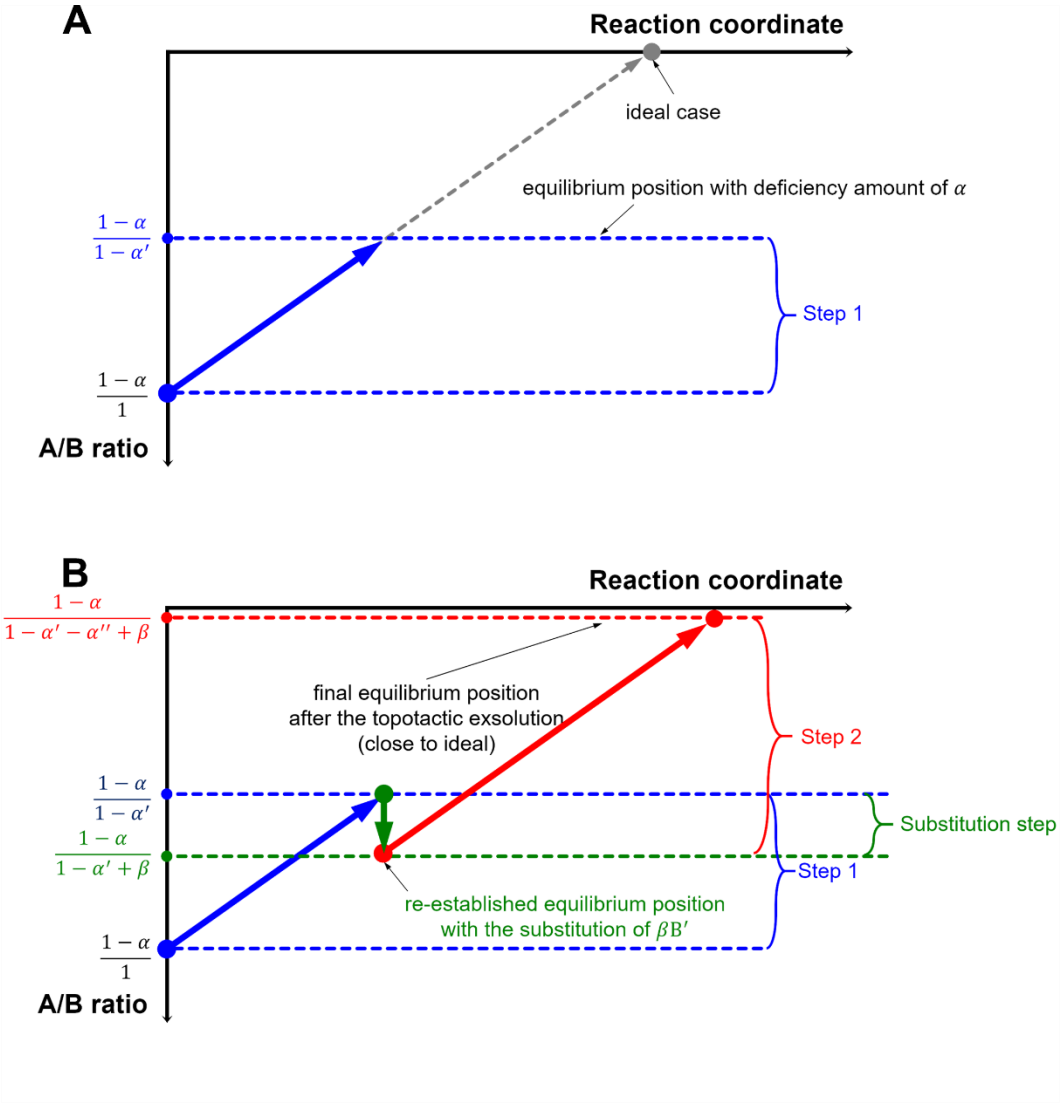

Fig. S1. A/B ratio for the exsolution pathway. (**A**) Conventional exsolution pathway with deficiency amount of α. (**B**) Topotactic exsolution pathway with re-established equilibrium position through the substitution step of Fe cation into Ni site.

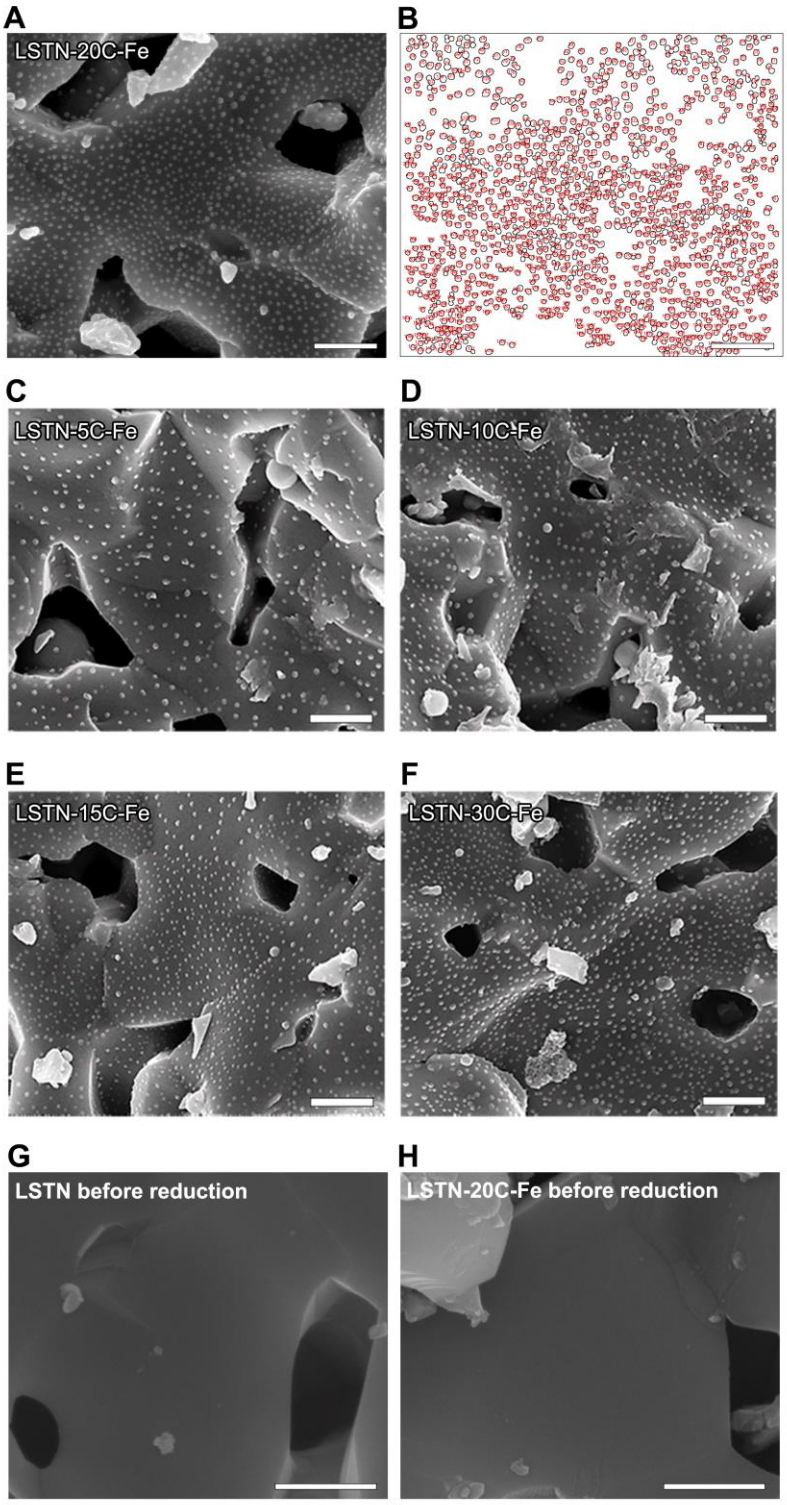

Fig. S2. Particle count analysis on the surface. (**A**) SEM image corresponding to Fig. 1D. (**B**) exsolved nanoparticles mapping and contour extracted with ImageJ from Supplementary Fig. 2A; scale bars are 500 nm. SEM images of (**C**) LSTN-5C-Fe, (**D**) LSTN-10C-Fe, (**E**) LSTN-15C-Fe,

and (**F**) LSTN-30C-Fe; scale bars are 500 nm. SEM images for (**G**) LSTN before reduction and (**H**) LSTN-20C-Fe before reduction; scale bars are 500 nm.

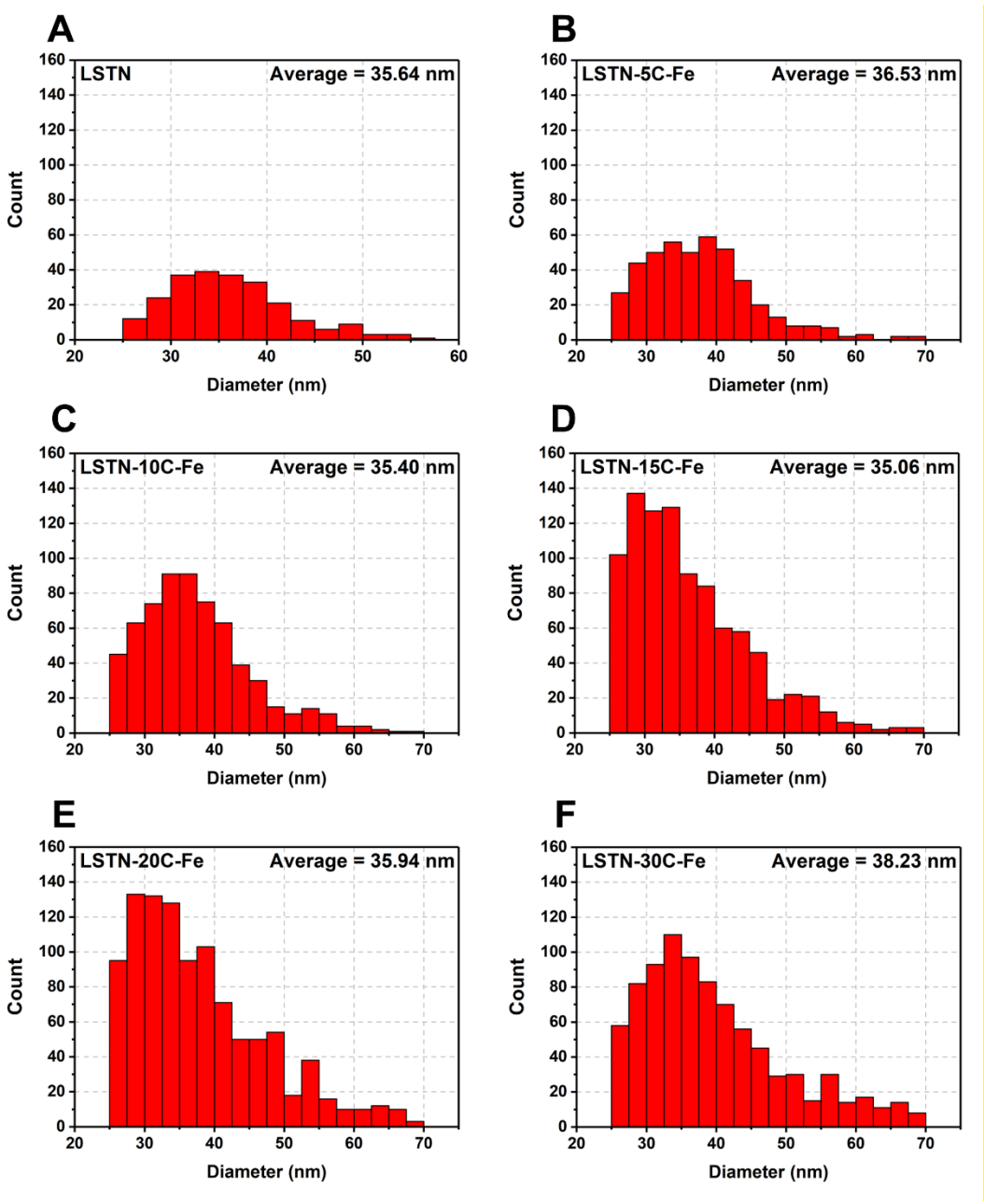

Fig. S3. Particle size distributions for the samples. The histogram of the particle size distribution for (**A**) LSTN, (**B**) LSTN-5C-Fe, (C) LSTN-10C-Fe, (D) LSTN-15C-Fe, (E) LSTN-20C-Fe, and (F) LSTN-30C-Fe.

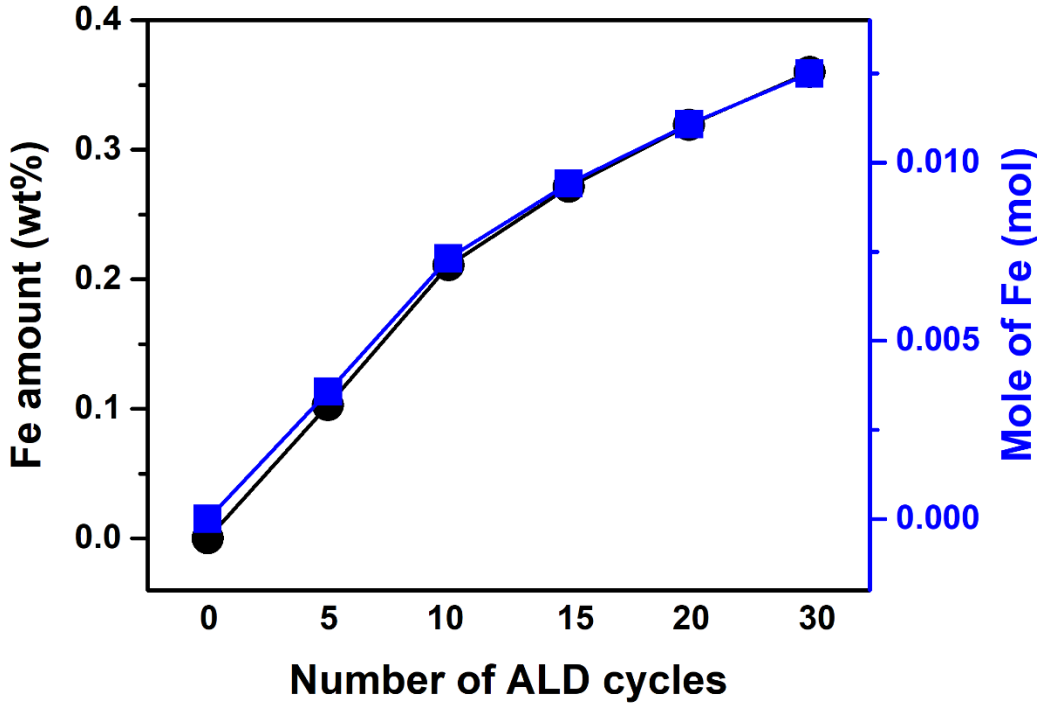

Fig. S4. Growth curves for ALD layers on LSTN powder. All measures were measured after thermal treatment to ensure the removal of moisture content.

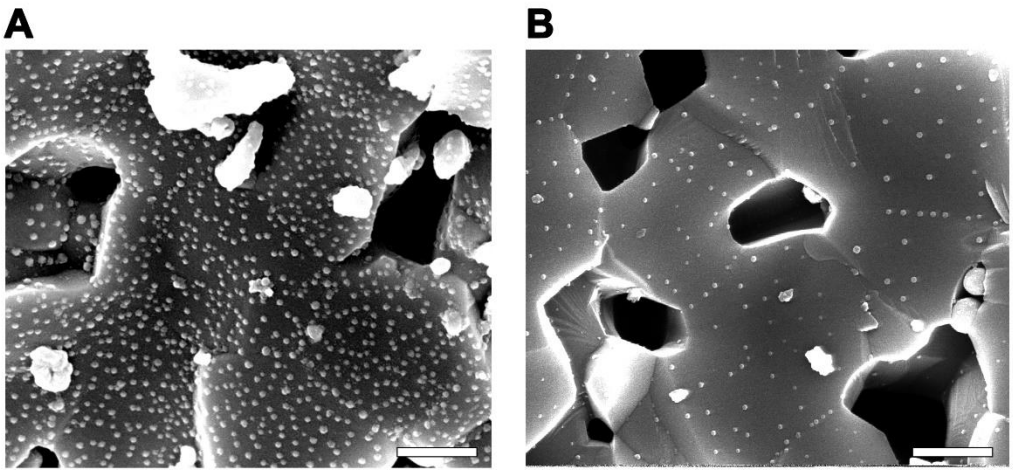

Fig. S5. SEM image of (**A**) LSTN-20C-Fe and (**B**) pristine LSTN reduced for 30 minutes; scale bars are 500 nm.

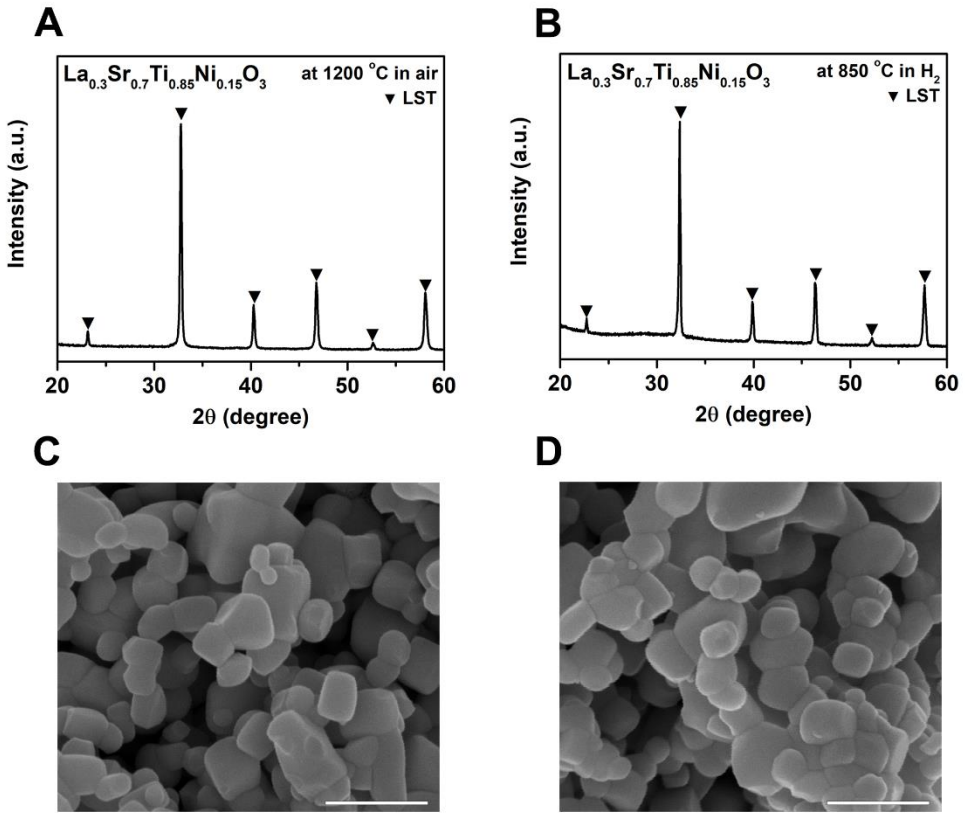

Fig. S6. X-ray diffraction patterns of (**A**) $La_{0.3}Sr_{0.7}Ti_{0.85}Ni_{0.15}O_3$ before reduction and (**B**) $La_{0.3}Sr_{0.7}Ti_{0.85}Ni_{0.15}O_3$ after reduction. SEM images of (**C**) $La_{0.3}Sr_{0.7}Ti_{0.85}Ni_{0.15}O_3$ before reduction and (**D**) $La_{0.3}Sr_{0.7}Ti_{0.85}Ni_{0.15}O_3$ after reduction; scale bars are 500 nm.

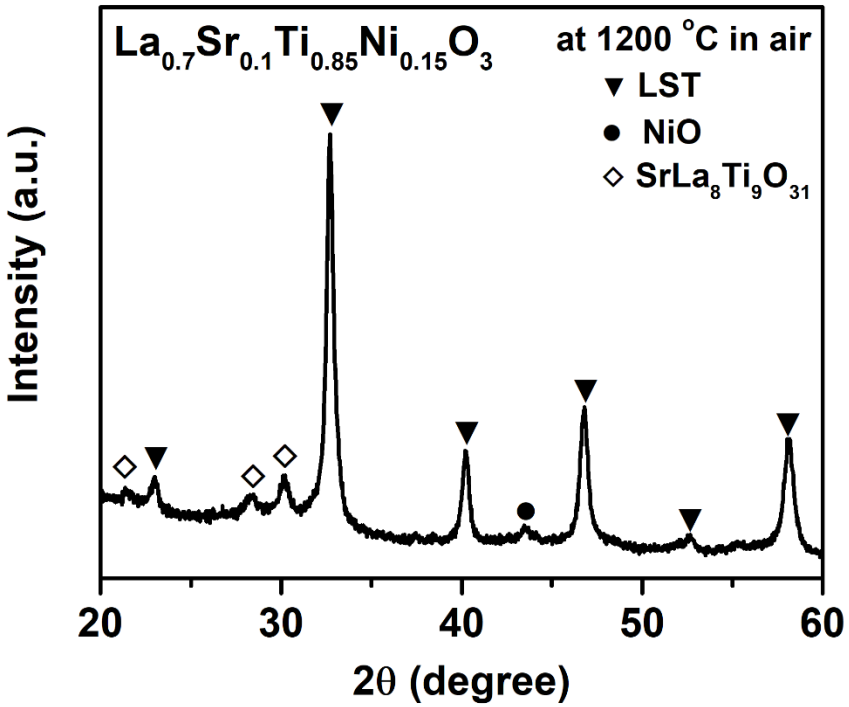

Fig. S7. X-ray diffraction patterns of $La_{0.7}Sr_{0.1}Ti_{0.85}Ni_{0.15}O_3$ before reduction.

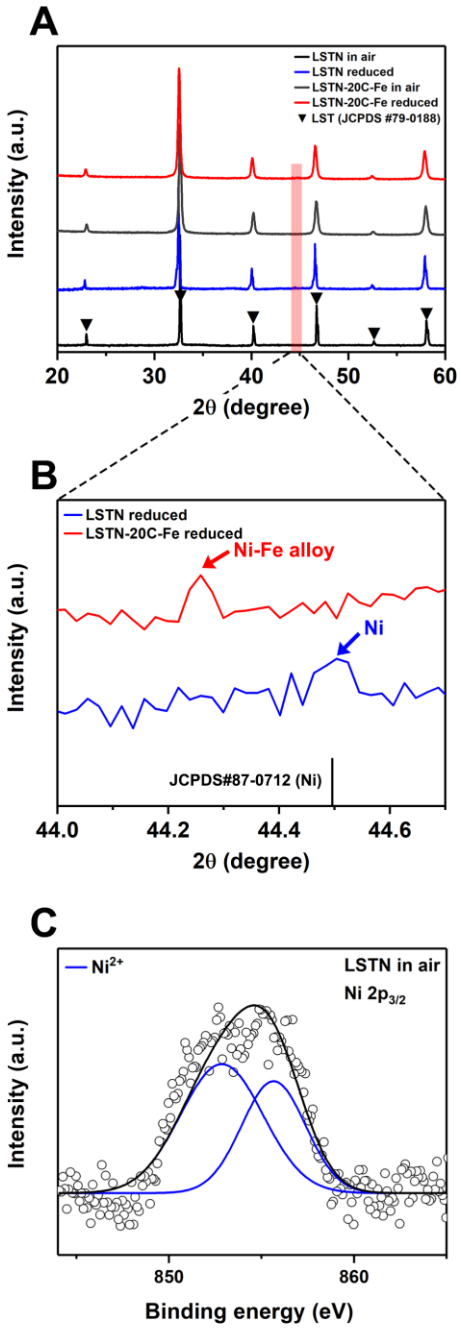

Fig. S8. X-ray diffraction patterns and X-ray photoelectron curves of the samples. X-ray diffraction patterns of (**A**) LSTN and LSTN-20C-Fe before/after reduction (red highlights around 44.5 º indicate exsolved metals) and (**B**) magnified metal peaks for LSTN and LSTN-20C-Fe. (**C**) X-ray photoelectron curves of LSTN before reduction.

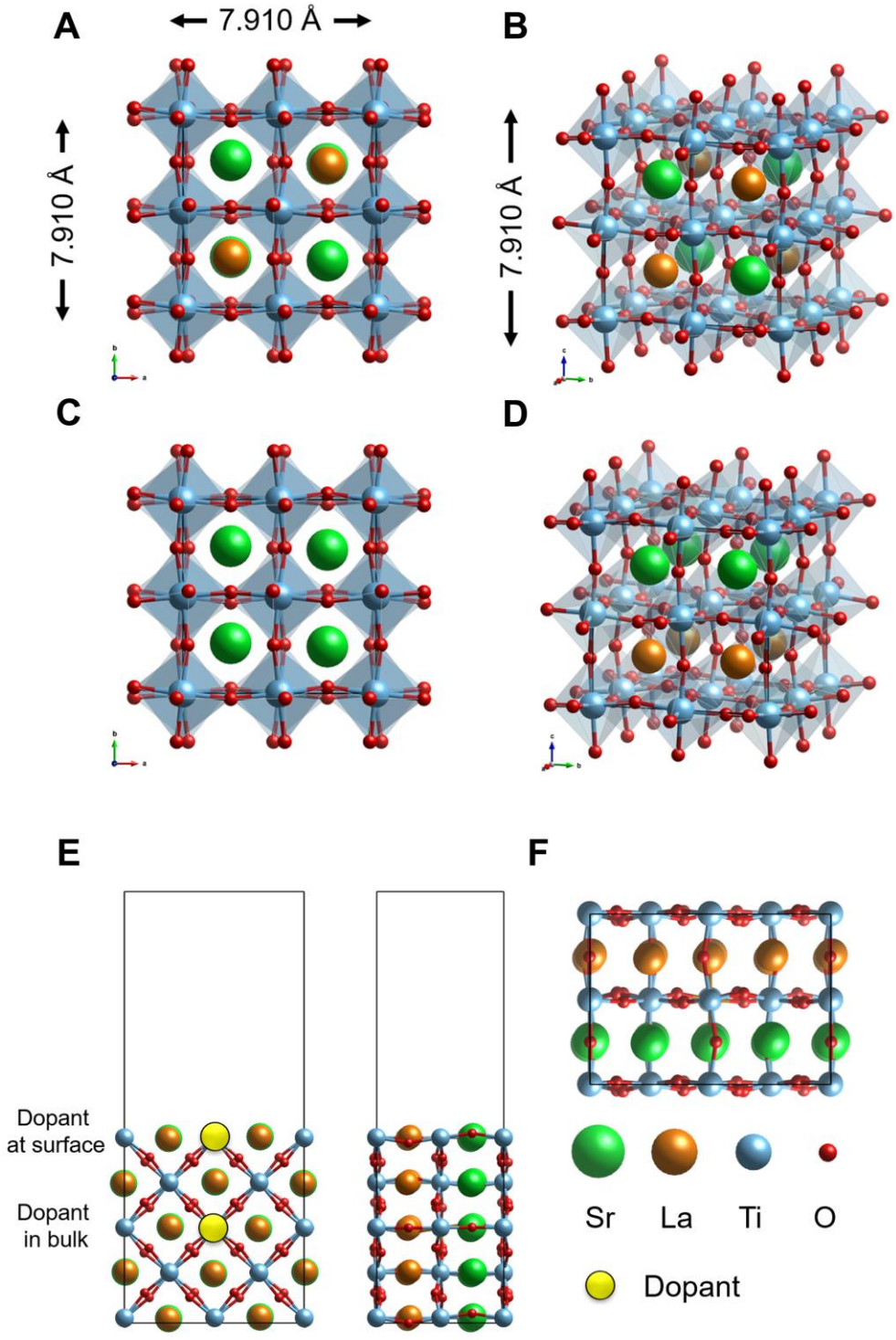

Fig. S9. Optimized two possible cation configurations of bulk structures of $La_{0.5}Sr_{0.5}TiO_3$. (**A**, **B**) and (**C**, **D**) represent top and side views of uniformly and layer by layer cation distributions, respectively. (**E**) side and (**F**) top views of optimized surface structure of $La_{0.5}Sr_{0.5}TiO_3(110)$ used for DFT calculations.

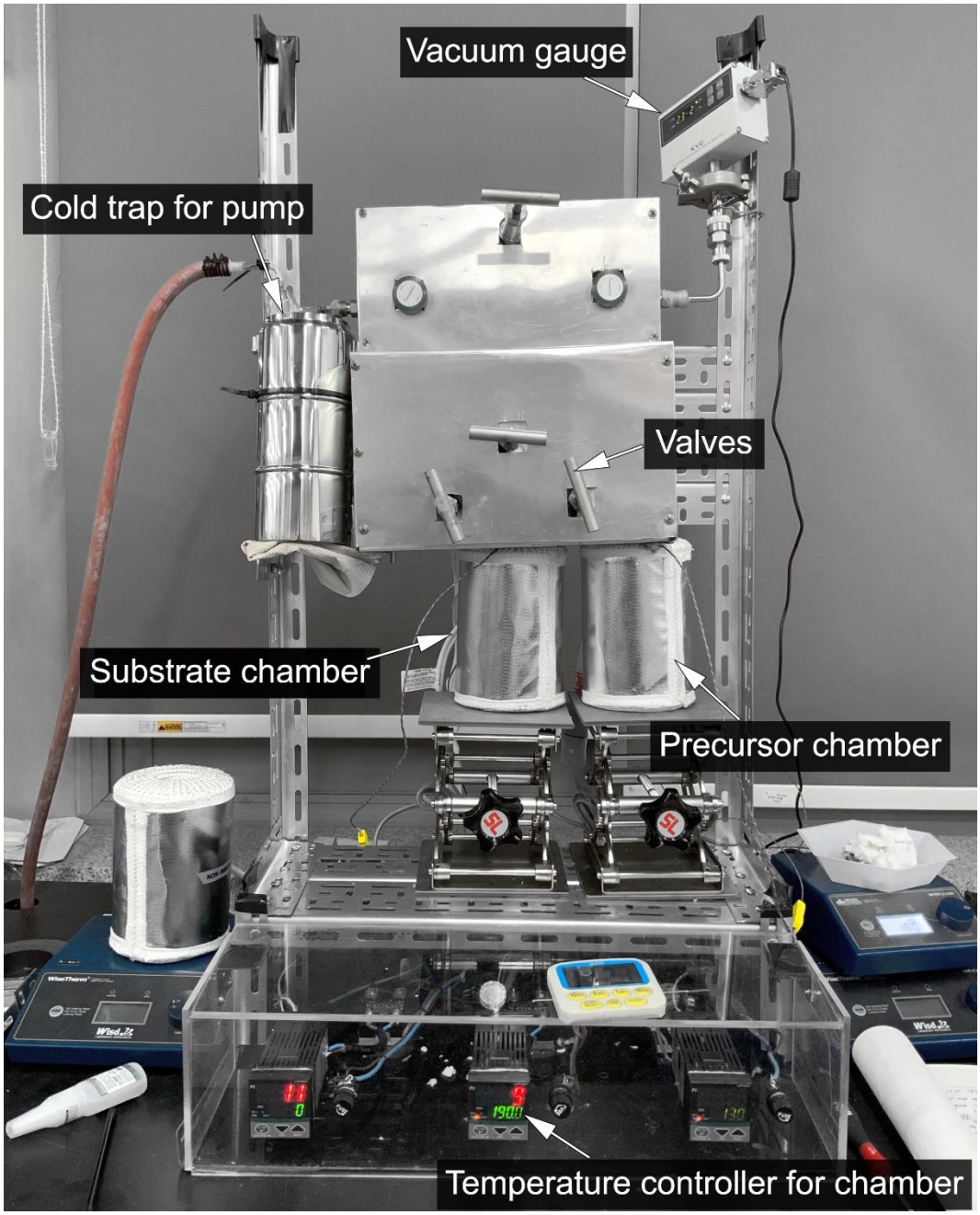

Fig. S10. A picture of home-made ALD apparatus. Photo Credit: Sangwook Joo, UNIST.